Journal of Magnetic Resonance **138,** 298–307 (1999)
Article ID jmre.1999.1750, available online at http://www.idealibrary.com on IDEAL®

Quadrupolar and Chemical Shift Tensors Characterized by 2D Multiple-Quantum NMR Spectroscopy

Ales Medek and Lucio Frydman[1]

Department of Chemistry (M/C 111), University of Illinois at Chicago, 845 West Taylor Street, Chicago, Illinois 60607-7061

Received November 2, 1998; revised February 24, 1999

The present work discusses a new 2D NMR method for characterizing the principal values and relative orientations of the electric field gradient and the chemical shift tensors of half-integer quadrupolar sites. The technique exploits the different contributions that quadrupolar and shielding interactions impart on the evolution of multiple-quantum and of single-quantum coherences, in order to obtain 2D powder lineshapes that are highly sensitive to these nuclear spin coupling parameters. Different spinning variants of this experiment were assayed, but it was concluded that a static version can yield the highest sensitivity to the values of the principal components and to the relative geometries of the local coupling tensors. It was found that correlating the central transition evolution with the highest available order of the spin coherence was also helpful for maximizing this spectral information. Good agreement between data obtained on ^{87}Rb ($S = \frac{3}{2}$) and ^{59}Co ($S = \frac{7}{2}$) samples and ideal theoretical lineshape predictions of this experiment was obtained, provided that heterogeneities in the multiple-quantum excitation and conversion processes were suitably accounted by procedures similar to those described in the spin-$\frac{1}{2}$ multiple-quantum NMR literature.

Key Words: **solid state NMR; half-integer quadrupole nuclei; multiple-quantum spectroscopy; 2D NMR correlations.**

1. INTRODUCTION

Quadrupolar nuclei with half-integer spin numbers ($S = \frac{3}{2}, \frac{5}{2}, \frac{7}{2}, \frac{9}{2}$) constitute the majority of magnetically active nuclides in the periodic table. Continuing interest in the solid state NMR spectroscopy of these isotopes is stimulated by the role that such elements play in many important materials such as minerals, ceramics, glasses, semiconductors, and catalysts. Unlike their more common spin-$\frac{1}{2}$ counterparts, quadrupolar nuclei interact not only with external and local magnetic fields but also with the field gradients that originate in the charges that surround the nuclear site (*1, 2*). These quadrupolar interactions are notably sensitive to the local electronic environment of an atomic site and nicely complement the insight made available by the shielding coupling tensor parameters.

In spite of the potential relevance that the combined measurement of these two interactions can have for the spectroscopic characterizations of electronic structures, NMR studies of quadrupolar nuclei are usually impaired by the broadenings that these anisotropies bring into the lineshapes of powdered samples. A common way to avoid the full broadening of the quadrupole interaction is to limit spectral observations to the central $-\frac{1}{2} \leftrightarrow +\frac{1}{2}$ transitions, devoid to first-order from quadrupolar interactions (*1–3*). Although free from the full quadrupole effects, these transitions may still enable the characterization of quadrupole couplings due to the presence of second-order shifts, as well as measurements of the chemical shift effects which will affect them in the usual spin-$\frac{1}{2}$ manner. Because of the combined effects of all these interactions the central transition spectra will depend on three parameters defining the shielding strength (isotropic chemical shift ν_0^{CS}, shift anisotropy δ_{CS}, and shielding asymmetry η_{CS}), on two parameters defining the local field gradients (quadrupolar coupling e^2qQ/h and quadrupole asymmetry η_Q) and on three Euler angles relating the principal axes systems (PASs) of those two tensors (*4–7*). Unfortunately, the determination of these eight independent parameters from a single spectral lineshape is usually ambiguous due to the similar effects that many of them have on defining the various singularities and inflexions characterizing the final powder pattern. We discuss here a novel approach based on two-dimensional multiple-quantum (2D MQ) NMR spectroscopy that, by establishing differential weightings among the contributions of shielding and quadrupole effects, can aid in discriminating these two interactions.

The possibility of distinguishing shielding from quadrupolar interactions in high-field central transition resonances arises from the fact that the former stems from a first-order effect while the latter arises from second-order ones. This opens a number of approaches to their spectral distinction. One of them is to exploit the different behavior that these shifts will exhibit upon varying the external magnetic field B_0, which will be linear (in Hertz) for the case of the shielding couplings but inversely proportional for the quadrupolar case (*1, 3*); this approach is fairly reliable provided that a large enough range of magnetic field strengths is available (*8*). A less straightforward but in many cases more amenable option is to exploit the different behavior that first- and

[1] To whom correspondence should be addressed at Department of Chemistry (M/C 111), University of Illinois at Chicago, 845 W. Taylor Street, Room 4500, Chicago, IL 60607-7061. Fax: (312) 996-0431. E-mail: lucio@samson.chem.uic.edu.

1090-7807/99 $30.00

second-order effects show when rotated with respect to the external magnetic field: the former ones will transform as second-rank tensors, while the latter ones will do so as fourth-rank representations (*9–11*). This distinction is central to many single crystal and variable angle spinning 1D NMR characterizations of quadrupole and shielding parameters (*12–14*).

Recently, it has also been shown that these different rotational behaviors can be incorporated into certain forms of multidimensional NMR which can separate shielding and quadrupolar interactions more efficiently than their unidimensional counterparts (*15, 16*). At the heart of these novel 2D and 3D powder NMR determinations lies the use of dynamic-angle spinning (DAS) (*17, 18*), a technique that, by correlating the spin evolution at two different spinning angles with respect to B_0, allows one to distinguish second- from fourth-rank anisotropies. Despite the potential demonstrated by these multidimensional experiments to disentangle shielding and quadrupole tensors, the technical complications generated by their reliance on sudden sample reorientations have apparently limited their routine chemical applications. Similar complications had been invoked in connection with the application of 2D DAS techniques toward the acquisition of high-resolution solid state quadrupole spectra. It has been shown, however, that many of these difficulties could be avoided by departing from the sole observation of the central NMR transitions and including into the spin evolution higher $-m \leftrightarrow +m$ symmetric transitions (*19, 20*). Since the resulting multiple-quantummagic-angle-spinning (MQ MAS) techniques became of common use (*21–33*), we and others have been exploring the possibility of extending the principles of these high-resolution methods to the task of distinguishing the shielding and second-order quadrupolar anisotropies affecting nuclear sites in random powders (*34–36*). This paper presents a written account of our findings in this area. It is shown that of all the possible acquisition alternatives, the clearest way to characterize the quadrupolar and shift anisotropies involves correlating the highest $-S \leftrightarrow +S$ MQ transition in the spin manifold with the $-\frac{1}{2} \leftrightarrow +\frac{1}{2}$ central transition while keeping the sample stationary. By contrast to what usually happens along the anisotropic dimension of MQ MAS experiments, however, simulating the 2D lineshapes arising from this nonspinning choice requires accounting for inhomogeneities in the MQ excitation and conversion processes. Experimental examples involving three-, five-, and seven-quantum (3Q, 5Q, and 7Q) 2D correlation NMR experiments on ^{87}Rb and ^{59}Co salts are presented which validate these theoretical considerations.

2. THEORY

The system that will be considered here consists of an ensemble of half-integer quadrupolar spins, placed inside strong static magnetic field and subject to the effects of perturbing quadrupolar and shielding couplings. It will then be assumed that the evolution of the spins is governed by the total Hamiltonian (*1–3*)

$$\mathcal{H}_T = \mathcal{H}_Z + \mathcal{H}_Q + \mathcal{H}_{CS}, \qquad [1]$$

where

$$\mathcal{H}_Z = -\gamma B_0 S_z = -\nu_L S_z \qquad [2]$$

is the dominant Zeeman coupling between the nuclear spins and an external magnetic field B_0. The effects of the remaining local quadrupole ($\mathcal{H}_Q$) and chemical shift ($\mathcal{H}_{CS}$) interactions are most conveniently described before truncation in terms of irreducible spherical tensor operators (*37, 38*)

$$\mathcal{H}_i = C_i \sum_{l=0}^{2} \sum_{m=-l}^{+l} (-1)^m T^i_{lm} R^i_{l-m}, \qquad [3]$$

where C_i, T^i_{lm}, and R^i_{lm} denote the coupling constants, the spin, and the spatial dependencies characterizing the chemical shift or the quadrupolar interactions. Because of the fast precession introduced by the external magnetic field B_0 on the nuclear spins, only the secular terms in Eq. [3] will end up observable in the high-field NMR spectra. Such truncation can be carried out only to first order in the case of the relatively small shielding couplings, but needs to be extended up to second-order energy corrections with respect to quadrupole coupling frequencies $C_Q = e^2qQ/[4S(2S-1)h]$ in order to account for the latter's larger size (*1, 2*). These approximations result in

$$\mathcal{H}_{CS} \approx \mathcal{H}^{(1)}_{CS} = S_z \left[\nu_0^{CS} + \sqrt{\frac{2}{3}} R_{20}^{CS} \right], \qquad [4]$$

where ν_0^{CS} and R_{20}^{CS} represent isotropic and anisotropic chemical shifts contributions, and

$$\mathcal{H}_Q \approx \mathcal{H}^{(1)}_Q + \mathcal{H}^{(2)}_Q = \frac{2C_Q}{\sqrt{6}} [3S_z^2 - S(S-1)] R^Q_{20} - \frac{2C_Q^2}{\nu_L} \left\{ \begin{array}{l} R^Q_{2-2} R^Q_{22} S_z [2S(S+1) - 2S_z^2 - 1] \\ + R^Q_{2-1} R^Q_{21} S_z [4S(S+1) - 8S_z^2 - 1] \end{array} \right\}, \qquad [5]$$

which is the sum of the first- and second-order quadrupole effects $\mathcal{H}^{(1)}_Q$, $\mathcal{H}^{(2)}_Q$.

The spatial dependencies $\{R^i_{2m}\}_{m=-2-2}$ involved in these expressions of $\mathcal{H}_{CS}$ and $\mathcal{H}_Q$ can be conveniently described in terms of the principal spherical tensor elements $\{\rho^i_{2m}\}_{m=-2-2}$ characterizing the coupling tensors in their principal axes systems. The transformation that will then convert the principal components of each tensor into a reference system fixed with respect to B_0 (the Zeeman axis system—ZAS) can be written with the aid of Wigner rotation matrices as (*39*)

$$R^i_{2m} = \sum_{m'=-2}^{+2} \rho^i_{2m'} D^{(2)}_{m'm}(\Omega_i). \quad [6]$$

Given the fact that shielding and quadrupolar tensors are not necessarily coincident and that our analysis will consider the use of sample spinning, it is convenient to describe the sets $\{\Omega_i\}$ of Euler angles that are involved in this relation in terms of the successive transformations

$$\mathrm{PAS_{CS}} \xrightarrow{(\alpha,\ \beta,\ \gamma)} \mathrm{PAS_Q} \xrightarrow{(\varphi,\ \psi)} \mathrm{RAS} \xrightarrow{(\omega_r t,\ \theta,\ 0)} \mathrm{ZAS}, \quad [7]$$

where the first rotation (α, β, γ) defines the relative orientations between the two nuclear coupling PASs, the second one relates the quadrupole tensor to a rotor-fixed axis system (RAS), and the last rotation relates this system to the Zeeman frame via a time-dependent transformation that contains the angle θ of sample spinning.

Equipped with these expressions it becomes possible to calculate the effects that quadrupole and chemical shift couplings are going to introduce on any of the Zeeman eigenstates. Of the different NMR transitions that could then potentially be monitored within the nuclear spin, manifold attention will be focused on the symmetric $-m \leftrightarrow +m$ ones, since owing to the quadratic dependence of $\mathscr{H}^{(1)}_{\mathrm{Q}}$ on S_z^2 their coherences will be the only ones that will evolve free from first-order quadrupole broadenings. To better appreciate the ways in which local couplings will affect these symmetric transitions, it is then convenient to express these $\nu_{-m\leftrightarrow+m}$ frequencies in terms of the various interactions and ranks which contribute to them (*19, 40, 41*). When disregarding the time-dependencies arising from the spinning-induced oscillatory terms, this results in the five-term frequency expression

$$\begin{aligned}\nu_{-m\leftrightarrow m} = {} & 2m\nu_0^{\mathrm{CS}} \\ & + \mathrm{C}_0^{\mathrm{S}}(m)\,\nu_0^{\mathrm{Q}} \\ & + 2mP_2(\cos\theta)\,\nu_2^{\mathrm{CS}}(\alpha,\ \beta,\ \gamma,\ \varphi,\ \psi) \\ & + C_2^{\mathrm{S}}(m)\,P_2(\cos\theta)\,\nu_2^{\mathrm{Q}}(\varphi,\ \psi) \\ & + C_4^{\mathrm{S}}(m)\,P_4(\cos\theta)\,\nu_4^{\mathrm{Q}}(\varphi,\ \psi)\end{aligned} \quad [8]$$

zero-rank (isotropic) chemical shift
zero-rank (isotropic) quadrupole shift
second-rank (anisotropic) chemical shift
second-rank quadrupole anisotropy
fourth-rank quadrupole anisotropy.

In this equation

$$P_2(\cos\theta) = (3\cos^2\theta - 1)/2 \quad [9a]$$

$$P_4(\cos\theta) = (35\cos^4\theta - 30\cos^2\theta + 3)/8 \quad [9b]$$

are second- and fourth-order Legendre polynomials scaling the anisotropies because of the sample spinning,

$$C_0^{\mathrm{S}}(m) = 2m[S(S+1) - 3m^2] \quad [10a]$$

$$C_2^{\mathrm{S}}(m) = 2m[8S(S+1) - 12m^2 - 3] \quad [10b]$$

$$C_4^{\mathrm{S}}(m) = 2m[18S(S+1) - 34m^2 - 5], \quad [10c]$$

are coefficients depending on the spin number S and transition order m which scale the various ranks of the quadrupolar contribution, and the explicit forms of the various frequencies involved are

$$\nu_0^{\mathrm{Q}} = -\frac{(e^2qQ/h)^2(3+\eta_{\mathrm{Q}}^2)}{10\nu_{\mathrm{L}}[2S(2S-1)]^2} \quad [11a]$$

$$\begin{aligned}\nu_2^{\mathrm{CS}}(\alpha,\ \beta,\ \gamma,\ \varphi,\ \psi) = \delta_{\mathrm{CS}}\Bigg\{ & \left[P_2(\cos\beta) - \frac{1}{2}\,\eta_{\mathrm{CS}}\sin^2\beta\cos 2\alpha\right]P_2(\cos\psi) \\ & -(3+\eta_{\mathrm{CS}}\cos 2\alpha)\,\frac{\sin 2\beta\,\sin 2\psi}{4}\cos(\gamma+\varphi) \\ & +\frac{1}{2}\,\eta_{\mathrm{CS}}\sin\beta\,\sin 2\alpha\,\sin 2\psi\,\sin(\gamma+\varphi) \\ & +\left[\frac{3}{4}\sin^2\beta - \frac{1}{4}\,\eta_{\mathrm{CS}}(\cos^2\beta+1)\cos 2\alpha\right] \\ & \times \sin^2\psi\,\cos(2\gamma+2\varphi) \\ & +\frac{1}{2}\,\eta_{\mathrm{CS}}\cos\beta\,\sin 2\alpha\,\sin^2\psi\,\sin(2\gamma+2\varphi)\Bigg\}\end{aligned} \quad [11b]$$

$$\nu_2^{\mathrm{Q}}(\varphi,\ \psi) = \frac{1}{288\nu_0}\left[\frac{e^2qQ}{S(2S-1)h}\right]^2\left[S(S+1) - \frac{3}{4}\right] \times \left[F_2(\varphi,\ \psi) - \frac{1}{7}\,F_1(\varphi,\ \psi)\right] \quad [11c]$$

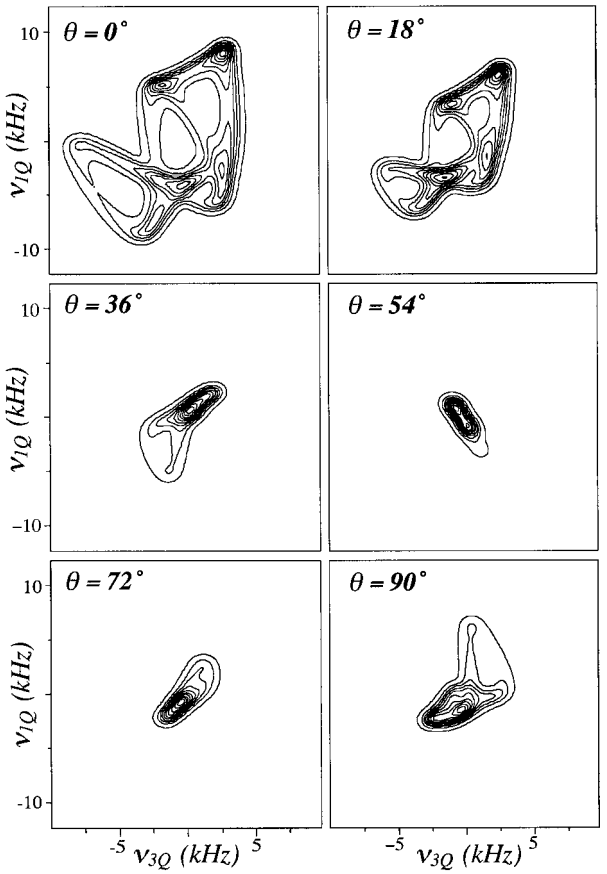

FIG. 1. Triple-/single-quantum 2D correlation NMR spectra calculated for a single $S = \frac{3}{2}$ site undergoing fast macroscopic rotation as a function of the spinning angle θ. The shielding and quadrupole parameters assumed for this site were $\nu_L = 98$ MHz, $e^2qQ/h = 3.3$ MHz, $\eta_Q = 0.2$, $\delta_{CS} = -15$ ppm, $\eta_{CS} = 0.6$, $\alpha = 90°$, $\beta = 30°$, $\gamma = 90°$; in all cases a Gaussian line broadening of 1 kHz was applied, and orientation-independent efficiencies for the MQ excitation and conversion processes were assumed.

and

$$\nu_4^Q(\varphi, \psi) = \frac{1}{3360\nu_0}\left[\frac{e^2qQ}{S(2S-1)h}\right]^2 \times \left[S(S+1) - \frac{3}{4}\right] F_1(\varphi, \psi), \qquad [11d]$$

with

$$F_1(\varphi, \psi) = \frac{35}{4}(3 - \eta_Q\cos 2\varphi)^2\sin^4\psi - 5(18 + \eta_Q^2 - 9\eta_Q\cos 2\varphi)\sin^2\psi + 18 + \eta_Q^2 \qquad [12a]$$

TABLE 1

Dependence of the Second- and Fourth-Rank Quadrupolar Scaling Coefficients on the $-m \leftrightarrow +m$ Coherence Order for Different Spin Numbers S

		Rank	
Spin number	Coherence order	$C_2^S(m)$	$C_4^S(m)$
$\frac{3}{2}$	1	24	54
$\frac{3}{2}$	3	0	−42
$\frac{5}{2}$	1	64	144
$\frac{5}{2}$	3	120	228
$\frac{5}{2}$	5	−40	−300
$\frac{7}{2}$	1	120	270
$\frac{7}{2}$	3	288	606
$\frac{7}{2}$	5	240	330
$\frac{7}{2}$	7	−168	−966
$\frac{9}{2}$	1	192	432
$\frac{9}{2}$	3	504	1092
$\frac{9}{2}$	5	600	1140
$\frac{9}{2}$	7	336	168
$\frac{9}{2}$	9	−432	−2232

$$F_2(\varphi, \psi) = \frac{5}{4}(3 - \eta_Q\cos 2\varphi)^2\sin^4\psi - 9(1 - \eta_Q\cos 2\varphi)\sin^2\psi + \eta_Q^2(\cos^2\psi - \sin^2\psi). \qquad [12b]$$

A full description of the quadrupolar and chemical shift interaction tensors requires the characterization of these vari-

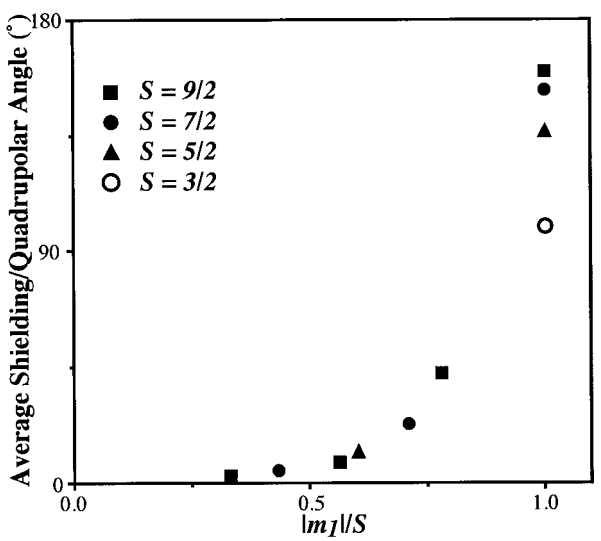

FIG. 2. Dependence of the average angle subtended between the shielding and the second-order quadrupole anisotropies in a 2D MQ NMR correlation spectrum, as a function of the coherence order m_1 chosen for the MQ evolution. Unidimensional NMR experiments would be characterized by an average angle of 0° for all spin numbers S.

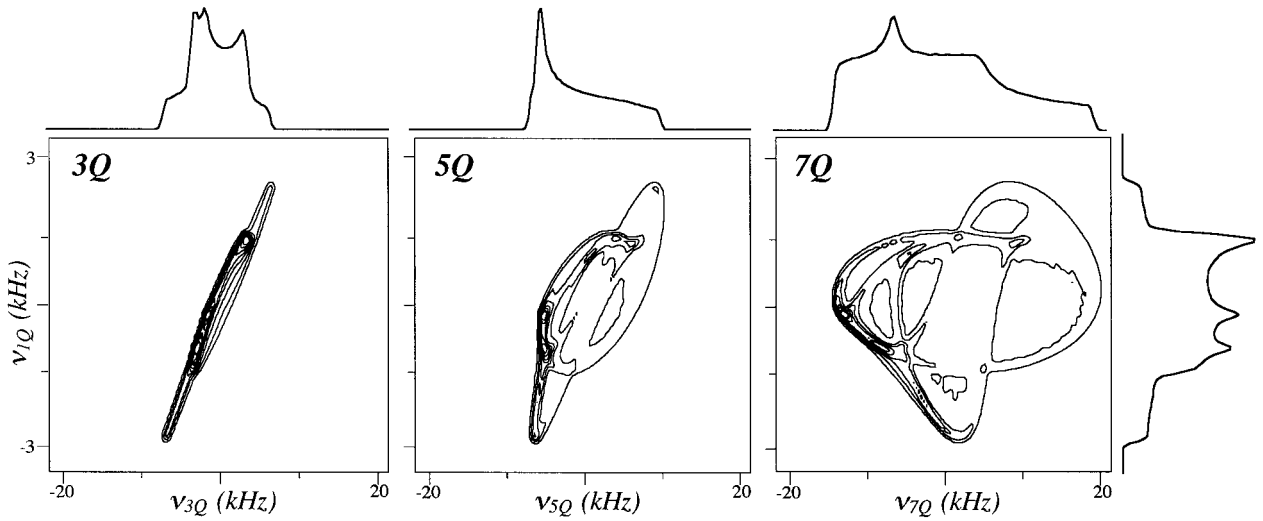

FIG. 3. Dependence of 2D MQ static NMR spectra on the m_1 coherence order employed in the correlation. These simulations assumed a spin-$\frac{7}{2}$ site with $\nu_L = 119$ MHz, $e^2qQ/h = 6$ MHz, $\eta_Q = 0.5$, $\delta_{CS} = 50$ ppm, $\eta_{CS} = 0.3$, Euler angles $(\alpha, \beta, \gamma) = (90°, 90°, 0°)$, 1 kHz Gaussian line broadening, and no orientation-dependent excitation or conversion distortions. The 1D traces illustrate the spectral projections along the various dimensions.

ous frequency terms, as well as a determination of the isotropic chemical shift ν_0^{CS}. As discussed in the Introduction this goal can be conveniently achieved by performing 2D NMR experiments where the various contributions to this otherwise overtly complex frequency domain expression are inequivalently weighted along the different dimensions. This has been done by circumscribing observations to the central $-\frac{1}{2} \leftrightarrow +\frac{1}{2}$ transition ($m = \frac{1}{2}$), and then switching the angle of sample spinning between two values θ_1 and θ_2 so as to differently scale the different ranks of the intervening anisotropies (*15, 16*). The alternative that we would like now to discuss involves keeping the angle of sample spinning constant and correlating instead the evolution among different coherence orders m_1 and m_2: chemical shifts will then scale simply as $2m$, while quadrupole effects will do so according to the $\{C_i^S(m)\}_{i=0-4}$ coefficients. Signal observation will in this case have to be constrained to $m_2 = \frac{1}{2}$ due to the need to directly detect voltages arising from single quantum magnetizations, but this still leaves open the possibility of choosing different experimental spinning angles and—for the case of higher spin numbers—different m_1 values along the indirect dimension.

A careful selection of the spinning angle θ appears important to achieve featured 2D NMR lineshapes that shall be sensitive with respect to the various nuclear coupling parameters involved. For instance it is clear that data collected while executing MAS will contain quadrupolar and isotropic chemical shift information, but no insight regarding the chemical shift anisotropy. In order to better appreciate the effects that changing the orientation of the spinning angle will have on the information available from 2D MQ NMR spectra, Fig. 1 illustrates a series of simulations of the results that these experiments should yield for triple-/single-quantum correlation acquisitions as calculated using Eqs. [8]–[12] for a single-site spin-$\frac{3}{2}$ powder. For the sake of simplicity high spinning speeds were assumed, and coupling, line broadening, and external magnetic field parameters similar to those characterizing some of the rubidium NMR analyses discussed later in this work were considered. At least judging by the dispersion in spectral features observed along the two frequency domains these simulations suggest that the highest experimental sensitivity toward the coupling parameters is achieved for $\theta = 0°$; that is, when avoiding sample spinning altogether. This static sample choice will in turn yield another practical advantage, related to the fact that no rotor-induced complications such as spinning sidebands will have to be considered.

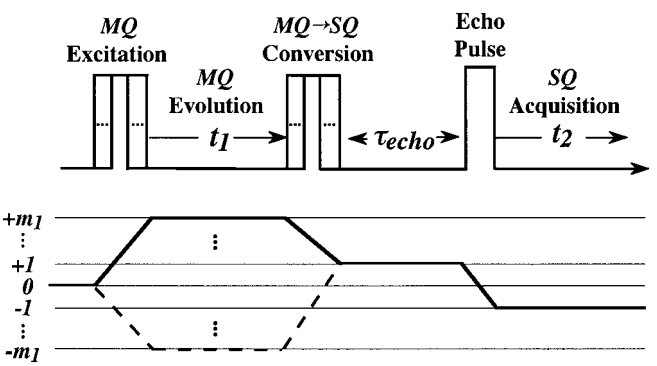

FIG. 4. Pulse sequence and schematic coherence pathway diagram employed in the 2D MQ correlation experiments. Excitation pulses were usually stepped over 8–10 values ranging between one-half and twice the optimum MQ pulse excitation length; 3–5 pulse values distributed in a similar fashion were employed for the conversion pulses. All these pulse length combinations were then phase cycled and coadded in the calculation of the final spectrum for the sake of minimizing nutational distortions (see text). Echo times $\tau_{echo} \approx$ 50–100 μs were used to account for the receiver dead times of the spectrometers.

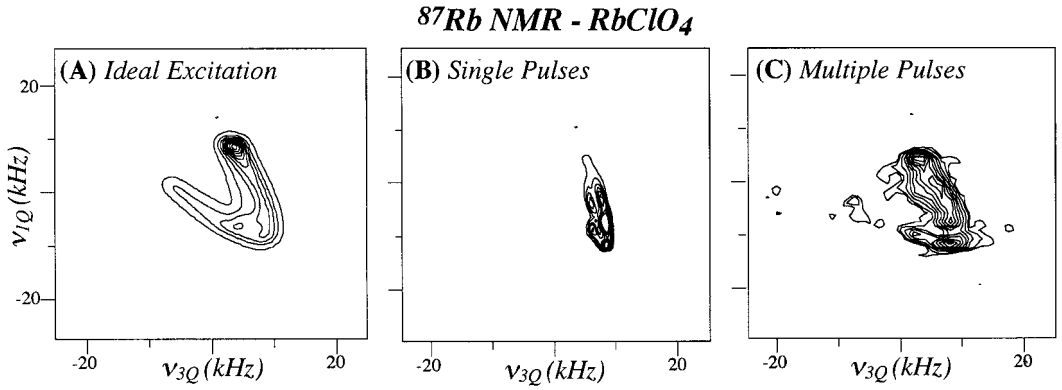

FIG. 5. Comparison between (A) an ideal triple-/single-quantum ^{87}Rb NMR correlation spectrum expected for static $RbClO_4$ on the basis of single crystal literature values (*14*), and experimental spectra acquired at 7.2 T using a single set (B) and a range (C) of MQ excitation and conversion pulse lengths. The spectrum in (B) was acquired using 3-μs MQ excitation and 1.4-μs conversion pulses; in (C) these values were swept between 1.5 and 5.7 μs and 0.8 and 2.0 μs in 0.6-μs increments, and the 24 resulting data sets were coadded prior to Fourier processing. Two hundred fifty-six and 128 scans per t_1 increment (40 t_1 points total) were employed in these experiments, leading to 3 and 34 h total acquisition times for the hypercomplex 2D sets in (B) and (C), respectively.

After settling on a selection of spinning conditions, a choice may remain for nuclei $S > \frac{3}{2}$ regarding which order of the multiple-quantum transition ($2m_1 = 3, 5, \ldots$) would be most convenient for the correlation experiment. Signal-to-noise considerations aside this choice should be dictated by the m_1 value that will differentiate best the quadrupolar and shielding contributions along the two spectral axes, since little would be gained over a conventional 1D NMR acquisition if the slopes subtended by the quadrupolar and shielding anisotropies in the 2D MQ spectrum are similar. This argument can be translated into more quantitative terms by noting that the slope that will characterize shielding powder patterns in these correlation spectra will be given by $2m_1$, while quadrupolar anisotropies will experience spin-dependent scaling factors $C_2^S(m_1)/C_2^S(\frac{1}{2})$, $C_4^S(m_1)/C_4^S(\frac{1}{2})$ (Eq. [10]). Although this implies that second- and fourth-rank quadrupole components will change differently with different choices of m_1, it is still possible to make approximate predictions on the usefulness of a particular m_1 choice by exploiting the fact that for a given spin S a change in MQ coherence order will introduce similar variations in both the C_2^S and C_4^S coefficients: both will tend to increase, decrease, and change of sign together (Table 1). It is thus reasonable to compare the shielding slope $2m_1$ in the 2D spectrum with an "average" slope $[C_2^S(m_1) + C_4^S(m_1)]/[C_2^S(\frac{1}{2}) + C_4^S(\frac{1}{2})]$ characterizing the quadrupole anisotropies and then investigate the extent to which these two interactions are differentiated by the choice in m_1. As summarized in Fig. 2, this criterion suggests that the optimum separation between the anisotropic quadrupolar and chemical shift contributions will be observed in experiments where the evolution of $-S \leftrightarrow +S$ MQ coherences is correlated with that of the central $-\frac{1}{2} \leftrightarrow +\frac{1}{2}$ transition. These qualitative arguments were also found to agree with a variety of numerical simulations carried out for several spin numbers; one such example is illustrated in Fig. 3. Further validations of these theoretical considerations as well as some of their practical limitations are presented with the experimental observations below.

3. EXPERIMENTAL SECTION

The theoretical predictions of the preceding paragraph were experimentally assayed on commercial compounds purchased from Aldrich and used without further purification. NMR spectra were acquired at magnetic fields of 7.2 and 11.8 T using SMIS (Surrey, UK) and laboratory-built NMR consoles respectively. Both spectrometers were fitted with laboratory-built probeheads capable of achieving radiofrequency (RF) nutation rates in excess of 150 kHz (7.2 T) and 120 kHz (11.8 T), as judged by the NMR nutation rates measured on 1 M aqueous solutions of $RbNO_3$ and $K_3[Co(CN)_6]$. These solutions were also used as external standards for referencing the solid state ^{87}Rb and ^{59}Co NMR measurements that were carried out. Figure 4 schematizes the pulse sequence used in the majority of the experiments. The first two pulses involve the excitation of MQ coherences and their subsequent conversion to single-quantum magnetizations, and in their implementation the highest available power was used. As further discussed in the next paragraph, the lengths of both the excitation and the conversion pulses had to be stepped throughout the experiments around their optimum efficiency values in order to diminish the influence of nutational distortions on the spectral lineshapes; in certain experiments up to 40 different pulse length combinations ended up being employed for each t_1 increment value. In order to overcome the effects of the spectrometer dead time and in view of the fast decay of the static powder signals, an additional 180° echo pulse (with typical length of 10 μs) was introduced in the direct acquisition dimension; all signals were thus acquired in an echo mode. Pure phase spectral lineshapes were achieved by means of hypercomplex data acquisition, with the correct coherence transfer pathways being selected

during t_1 by employing the appropriate RF phase combinations. 2D data acquisitions involved the collection of 128 t_2 points and 32–50 incremented t_1 values; during processing these were zero filled to 256 and 128 points, respectively. Thanks to the short longitudinal relaxation times of the metal sites that were analyzed, recycle delays of only 300–500 ms (^{87}Rb) and 100–150 ms (^{59}Co) could be employed throughout the bidimensional acquisitions; additional acquisition details are specified in the captions to the corresponding spectra. The resulting experimental data were processed off-line on a PowerPC using the RMN program (Prof. P. J. Grandinetti, Ohio State University); numerical simulations were performed on an SGI computer using a variety of C language programs.

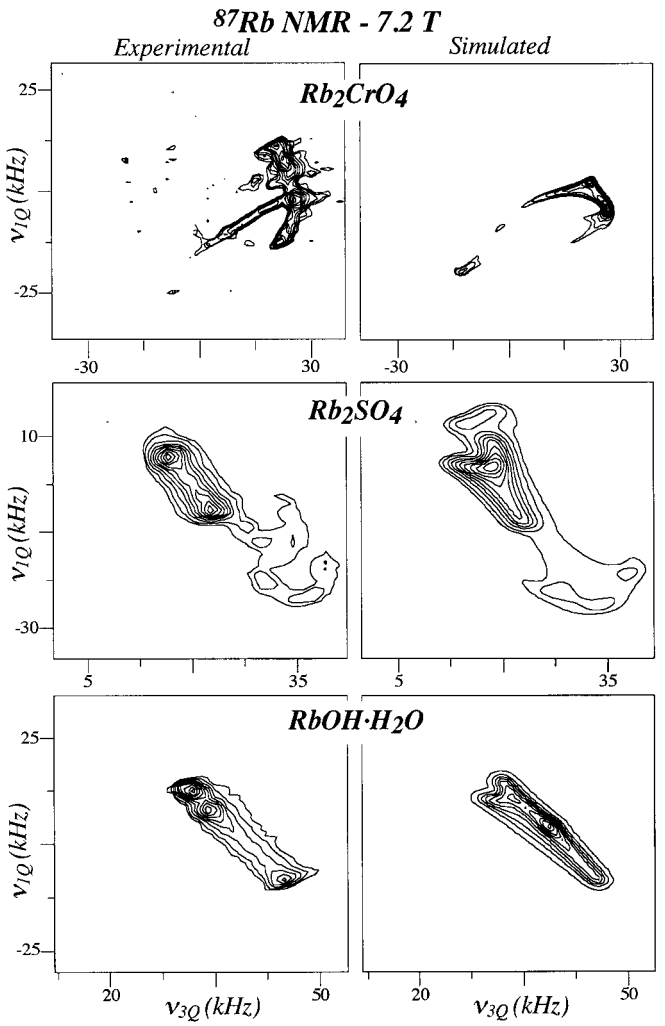

FIG. 6. Comparison between experimental triple-/single-quantum static ^{87}Rb NMR spectra recorded on the indicated salts at 7.2 T, and best-fit simulations resulting from the parameters summarized in Table 2. MQ excitation pulses were swept between 1.5 and 5.7 μs in 0.6-μs increments; conversion pulses were kept fixed at 1.2 μs for the perchromate and sulfate salts, but stepped over three values for the hydroxide (0.8, 1.4, 2.0 μs). In all experiments 0.5-s recycle delays and 32 t_1 points were employed, leading to total acquisition times of 28, 24, and 33 h, respectively. Simulations on the right do not consider excitation or conversion distortions, and since for Rb_2CrO_4 the MQ signal of one of its sites was incompletely excited under these conditions due to its large quadrupole coupling, it was not included in the calculations.

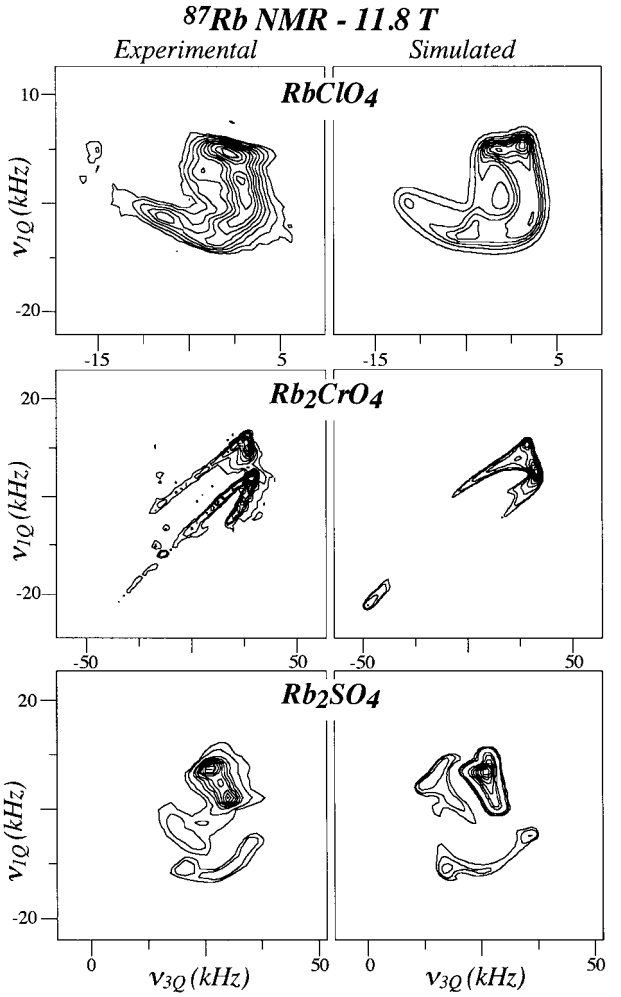

FIG. 7. Comparison between experimental 11.8 T ^{87}Rb 2D MQ static NMR spectra recorded on the indicated salts, and their best fit simulations. In all experiments excitation and conversion pulse lengths were swept between 1.5 and 12.0 μs and 1.0 and 8.0 μs in 1.5- and 1.75-μs steps, respectively, and for each of the resulting combinations 32 t_1 points were collected. Simulation considerations are as in Fig. 6.

4. RESULTS AND DISCUSSION

The potential applications of 2D MQ correlations toward the extraction of the anisotropic coupling parameters were explored on two different and easily accessible nuclei: ^{87}Rb ($S = \frac{3}{2}$, nat. abundance = 33%) and ^{59}Co ($S = \frac{7}{2}$, nat. abundance = 100%). Furthermore, spectra were acquired on samples for which at least some of the nuclear coupling parameters had previously been measured by alternative methods so as to test the reliability of the MQ static approach. Several spinning variants of the 2D MQ NMR experiments were assayed but, in

TABLE 2
Comparison between the Shielding and Quadrupolar Tensor Parameters Extracted by Iterative Fitting of 2D MQ Static Spectra (Figs. 5–8) and Literature Counterparts[a]

Compound	(e^2qQ/h) (MHz)	η_Q	δ_{CS} (ppm)	η_{CS}	ν_0^{CS} (ppm)	(α, β, γ)[b] (degrees)
$RbClO_4$ (MQ NMR)	3.3 ± 0.2	0.2 ± 0.2	−14 ± 3	0.6 ± 0.2	−14 ± 3	(90, 25, 0)
$RbClO_4$ (Ref. *14*)	3.30 ± 0.04	0.21 ± 0.03	−13.8 ± 1.5	0.61 ± 0.24	−13.7 ± 0.6	(94, 28, 87)
Rb_2CrO_4—site 1 (MQ NMR)	3.5 ± 0.2	0.3 ± 0.2	−110 ± 5	0.0 ± 0.2	−7 ± 3	(0, 40, 15)
Rb_2CrO_4—site 1 (Ref. *34*)	3.5	0.3	−110	0	−7	(0, 70, 0)
Rb_2SO_4—site 1 (MQ NMR)	2.7 ± 0.2	0.9 ± 0.2	−3 ± 3	0.3 ± 0.2	43 ± 3	(80, 20, 110)
Rb_2SO_4—site 1 (Ref. *14*)	2.72 ± 0.03	0.93 ± 0.03	−2.7 ± 0.9	0.26 ± 0.62	42.6 ± 0.3	(76, 17, 110)
Rb_2SO_4—site 2 (MQ NMR)	5.3 ± 0.2	0.1 ± 0.2	25 ± 3	0.5 ± 0.2	16 ± 3	(30, 40, 0)
Rb_2SO_4—site 2 (Ref. *14*)	5.29 ± 0.05	0.12 ± 0.03	25 ± 3	0.54 ± 0.30	15.5 ± 1.6	(9, 37, 270)
$RbOH \cdot H_2O$ (MQ NMR)	3.6 ± 0.2	0.6 ± 0.2	20 ± 5	0.6 ± 0.2	91 ± 5	(0, 0, 0)
$RbOH \cdot H_2O$ (Ref. *6*)	4.32	0.77	−115.76	0.42	30.5	(−21, 23, 48)
$K_3[Co(CN)_6]$ (MQ NMR)	6.0 ± 0.2	0.7 ± 0.2	−50 ± 5	0.3 ± 0.2	0 ± 3	(25, 70, 90)
$K_3[Co(CN)_6]$ (Ref. *46*)[c]	5.88 ± 0.01	0.9 ± 0.004	—	—	—	—

[a] Coupling parameters as defined in Eqs. [4]–[7] and in the cited literature.
[b] Average uncertainties of the MQ NMR angular values are (±15, ±10, ±30) degrees, as judged by departures from the experimental lineshapes.
[c] Shielding parameters not reported.

agreement with the theoretical predictions discussed earlier and with the experimental behavior reported by Pines and coworkers (*34*), limited correlations between the shielding and quadrupolar tensors could be obtained for most spinning angles. Only acquisitions on static samples are therefore discussed in detail.

Upon collecting static 2D NMR correlation spectra with all pulses set to their optimized MQ powder excitation and conversion efficiencies (*42*), notable deviations from the ideal lineshapes were observed (Fig. 5). These distortions were traced to nutational effects of the excitation and conversion pulses, which provide signals of different crystallites with intensities that do not correspond to their ideal and *a priori* equal values. These distortions are usually minor in MQ MAS NMR experiments due to the compensating effects arising from sample spinning (*20*), but are known to affect other types of static MQ NMR experiments such as those involving dipole-coupled spin-$\frac{1}{2}$ networks in oriented or solid phases (*43, 44*). Based on protocols that have been developed to deal with this type of MQ spin-$\frac{1}{2}$ problems (*45*), a procedure was devised for their compensation by means of the coaddition into a final spectrum of acquisitions carried out using a range of MQ excitation and conversion pulses (Fig. 5C). Then, even though any individual combination of pulse durations led to some spectral distortions, spectra that were to a large extent free from nutational effects resulted after adding up all these data. This in turn allowed us to account for the MQ excitation distortions without having to go through the complete propagation of the spin evolution throughout the various stages of the experiment, thus providing a simple method to analyze these kinds of data.

Figures 6 and 7 show experimental 2D MQ static correlation spectra acquired in this manner for different rubidium salts at magnetic field strengths of 7.2 and 11.8 T. Also shown in these figures are best fit simulations of the data assuming ideal excitation and conversion processes. To retrieve these fittings the ^{87}Rb parameters available from the literature were used as a starting point and subsequently varied in an attempt to obtain the closest possible match to the variable field 2D MQ NMR features. This search involved iterating on all the coupling parameters simultaneously and led to the full sets of nuclear coupling constants summarized in Table 2. Error brackets in these values denote the intervals outside which unacceptably large differences resulted between calculations and experiments, as judged on the basis of simple visual comparisons. In general the MQ results matched well the literature values, with major discrepancies usually confined to the Euler angles that relate quadrupole and shielding tensors. It is yet unclear where these disagreements stem from; potential origins include differences in the conventions used to describe the angular transformations or residual MQ nutation distortions that were unaccounted for by the variable pulse width acquisition protocol.

Finally, the effects described in the preceding section regarding how changes in the coherence order m_1 will affect MQ correlation spectra were explored by collecting 3Q, 5Q, and 7Q 2D NMR data on a $K_3[Co(CN)]_6$ powdered sample. Figure 8 shows the various 2D ^{59}Co NMR traces obtained using an external B_0 field of 11.8 T and compares them with spectra simulated so as to obtain the best agreement with the 1D and 2D information (Table 2). A good match is again obtained for all the coherence orders even if assuming ideal MQ excitation and conversion processes, while the data exemplify the gain in features that occurs as higher orders of coherence are employed in the correlations. Still it should be mentioned that the efficiencies of high-quanta excitation and conversion processes can be considerably smaller than those of simple SQ excita-

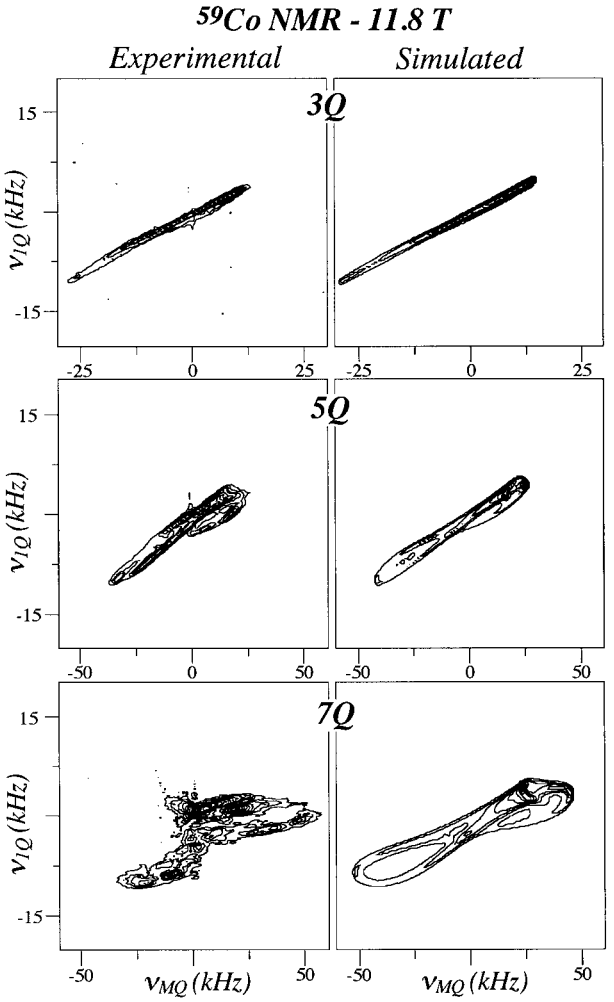

FIG. 8. Comparison between experimental spectra and best-fit simulations of ^{59}Co MQ static correlations acquired on $K_3[Co(CN)_6]$ as a function of the coherence order m_1. Data were collected at 11.8 T using the 40 excitation/conversion pulse length combinations described in Fig. 7, as well as 32 t_1 points for each hypercomplex data set. The 3Q, 5Q, and 7Q correlation experiments involved the collection of 48, 240, and 480 scans/t_1 point, leading to total acquisition times of 4, 19, and 38 h, respectively.

tions, and therefore even slight instrumental imperfections during the course of a conventional phase cycle might result in some artifacts in the final spectra. In this respect it is likely that the advent of gradient-enhanced spectroscopy methods might proove highly beneficial for the implementation of this type of experiments (*28*).

5. CONCLUSIONS

The present work demonstrates the use of 2D multiple-quantum NMR techniques for extracting detailed information about the nuclear coupling parameters characterizing half-integer quadrupolar spins, particularly their chemical shift and field gradient anisotropies and the relative orientations between these two tensors. The highest sensitivity of 2D MQ NMR to these coupling parameters was found in static experiments where the highest multiple-quantum $-S \leftrightarrow +S$ order available in the manifold was correlated with the single-quantum evolution. The resulting 2D spectra allowed us to obtain the nuclear coupling parameters by iterative numerical fittings of the ideal lineshapes, provided that distortions arising from nutations were compensated at least in a partial way by coadding data sets acquired using slightly different pulse lengths. Minor differences between the experimental MQ spectra and ideal lineshapes, however, still remained, which can probably be accounted for completely only by computing a full quantum mechanical propagation of the spin system throughout the different stages of the experiment. The resulting numerical procedure might eventually endow the MQ static technique with an analytical capability comparable to that of single crystal determinations, while remaining free from some of the latter's practical complications.

In spite of its simplicity and rich spectral information, the MQ static method as was here described is prone to suffer from a number of limitations. The most notable ones are its low resolution nature and the complications which may arise from strong dipole–dipole interactions. The latter could be coped with easily if they are heteronuclear with standard spin decoupling techniques, but will remain problematic if they are homonuclear in nature. Site resolution problems, on the other hand, might be alleviated while preserving the simplicity of the experiment by extensions which employ variable-angle-spinning and/or three-dimensional acquisitions; these and related research avenues are currently being explored.

ACKNOWLEDGMENTS

We are grateful to the Amoco Corporation for the donation of the 7.2 T SMIS NMR spectrometer. This work was supported by the National Science Foundation through Grants DMR-9806810 and CHE-9841790 (Creativity Extension Award). A.M. acknowledges UIC for a Dean Fellowship; L.F. is a Beckman Young Investigator (1996–1998), Camille Dreyfus Teacher–Scholar (1996–2001), University of Illinois Junior Scholar (1997–2000), and Alfred P. Sloan Fellow (1997–2000).

REFERENCES

1. M. H. Cohen and F. Reif, *Solid State Phys.* **5,** 321 (1957).
2. D. Freude and J. Haase, *NMR Basic Prin. Prog.* **29,** 1 (1993).
3. A. Abragam, "The Principles of Nuclear Magnetism," Oxford Univ. Press, Oxford (1985).
4. K. Narita, J. J. Umeda, and H. Kusumoto, *J. Chem. Phys.* **44,** 2719 (1966).
5. P. J. Chu and B. Gerstein, *J. Chem. Phys.* **94,** 2081 (1989).
6. J. T. Cheng, J. C. Edwards, and P. D. Ellis, *J. Phys. Chem.* **94,** 553 (1990).
7. W. P. Power, R. E. Wasylishen, S. Mooibroek, B. A. Pettitt, and W. Danchura, *J. Phys. Chem.* **94,** 591 (1990).

8. A. Medek, V. Frydman, and L. Frydman, *Proc. Natl. Acad. Sci. USA* **94,** 14237 (1997).
9. A. Llor and J. Virlet, *Chem. Phys. Lett.* **152,** 248 (1988).
10. E. W. Wooten, K. T. Muller, and A. Pines, *Acc. Chem. Res.* **25,** 209 (1992).
11. B. F. Chmelka and J. W. Zwanziger, *NMR Basic Prin. Prog.* **33,** 79 (1994).
12. E. Kundla, A. Samoson, and E. Lippmaa, *Chem. Phys. Lett.* **83,** 229 (1981).
13. S. Ganapathy, S. Schramm, and E. Oldfield, *J. Chem. Phys.* **77,** 4360 (1982).
14. T. Vosegaard, J. Skibsted, H. Bildsoe, and H. J. Jakobsen, *J. Magn. Reson. A* **122,** 111 (1996).
15. A. Medek, J. R. Sachleben, P. Beverwyk, and L. Frydman, *J. Chem. Phys.* **104,** 5374 (1996).
16. J. S. Shore, S. H. Wang, R. E. Taylor, A. T. Bell, and A. Pines, *J. Chem. Phys.* **105,** 9412 (1996).
17. B. Q. Sun, Ph.D. Thesis, Materials Science Division, Lawrence Berkeley Laboratory; Univ. of California, Berkeley (1991).
18. K. T. Mueller, B. Q. Sun, G. C. Chingas, J. W. Zwanziger, T. Terao, and A. Pines, *J. Magn. Reson.* **86,** 470 (1990).
19. L. Frydman and J. S. Harwood, *J. Am. Chem. Soc.* **117,** 5367 (1995).
20. A. Medek, J. S. Harwood, and L. Frydman, *J. Am. Chem. Soc.* **117,** 12779 (1995).
21. D. Massiot, B. Tonzo, D. Trumeau, J. P. Coutures, J. Virlet, P. Florian, and P. J. Grandinetti, *Solid State NMR* **6,** 73 (1996).
22. S.-J. Hwang, C. Fernandez, J. P. Amoureux, J. Cho, S. W. Martin, and M. Pruski, *Solid State NMR* **8,** 109 (1997).
23. C. Fernandez and J. P. Amoureux, *Chem. Phys. Lett.* **242,** 449 (1995).
24. G. Wu, D. Rovnyak, B. Sun, and R. G. Griffin, *Chem. Phys. Lett.* **249,** 210 (1996).
25. M. J. Duer and C. Stourton, *J. Magn. Reson.* **124,** 189 (1997).
26. S. P. Brown, S. J. Heyes, and S. Wimperis, *J. Magn. Reson. A* **119,** 280 (1996).
27. S. P. Brown and S. Wimperis, *J. Magn. Reson.* **124,** 279 (1997).
28. C. A. Fyfe, J. Skibsted, H. Grodney, and H. M. z. Altenschildesche, *Chem. Phys. Lett.* **281,** 44 (1997).
29. S. P. Brown and S. Wimperis, *J. Magn. Reson.* **128,** 42 (1997).
30. M. Hanaya and R. K. Harris, *J. Phys. Chem.* **A101,** 6903 (1997).
31. J. F. Stebbins and Z. Xu, *Nature* **364,** 60 (1998).
32. G. Wu, D. Rovnyak, P. C. Huang, and R. G. Griffin, *Chem. Phys. Lett.* **277,** 79 (1997).
33. S.-J. Hwang, C. Fernandez, J. P. Amoureux, J. W. Han, J. Cho, S. W. Martin, and M. Pruski, *J. Am. Chem. Soc.* **120,** 7337 (1998).
34. S. H. Wang, Z. Xu, J. H. Baltisberger, L. M. Bull, J. F. Stebbins, and A. Pines, *Solid State NMR* **8,** 1 (1997).
35. A. Medek and L. Frydman, 39th Rocky Mountain Conference in Analytical Chemistry—NMR Symposium, Poster 43, Denver, CO (1997).
36. J. P. Amoureux and C. Fernandez, personal communication (1997).
37. U. Haeberlen, "Advances in Magnetic Resonance," Supplement 1, Academic Press, New York (1976).
38. M. Mehring, "High Resolution NMR in Solids," Springer, Berlin (1983).
39. M. E. Rose, "Elementary Theory of Angular Momentum," Dover, New York (1995).
40. F. Lefebvre, J. P. Amoureux, C. Fernandez, and E. G. Derouane, *J. Chem. Phys.* **86,** 6070 (1987).
41. J. Skibsted, N. C. Nielsen, H. Bildsoe, and H. J. Jakobsen, *J. Magn. Reson.* **95,** 88 (1991).
42. J. P. Amoureux, C. Fernandez, and L. Frydman, *Chem. Phys. Lett.* **259,** 347 (1996).
43. G. Bodenhausen, *Prog. Nucl. Magn. Reson. Spectrosc.* **14,** 137 (1981).
44. K. Schmidt-Rohr, *Macromolecules* **29,** 3975 (1996).
45. S. Sinton and A. Pines, *Chem. Phys. Lett.* **76,** 263 (1980).
46. J. A. Lourens and E. C. Reynhardt, *Phys. Stat. Sol. (a)* **11,** 739 (1972).